Ceramics International xxx (xxxx) xxx–xxx

Contents lists available at ScienceDirect

Ceramics International

journal homepage: www.elsevier.com/locate/ceramint

Phase evolution and microwave dielectric properties of $SrTiO_3$ added $ZnAl_2O_4$–Zn_2SiO_4–SiO_2 ceramics

Xing Hu*, XinJie Huang, YuHui Chen, Yi Li, ZhiYuan Ling

Department of Electronic Materials Science and Engineering, South China University of Technology, Guangzhou, 510640, China

ARTICLE INFO

Keywords:
Microwave dielectric properties
Ceramic
Phase evolution

ABSTRACT

Phase evolution and microwave dielectric properties of $SrTiO_3$ added $ZnAl_2O_4$–$3Zn_2SiO_4$–$2SiO_2$ ceramics system were investigated. With the addition of $SrTiO_3$, the sintering temperature for dense ceramic is reduced from 1320 °C to 1180–1200 °C. According to the nominal composition $ZnAl_2O_4$–$3Zn_2SiO_4$–$2SiO_2$-y$SrTiO_3$, phase evolution is revealed by XRD patterns and Back Scattering Electron images: Zn_2SiO_4, $ZnAl_2O_4$ and SiO_2 phases coexist at y = 0; $SrTiO_3$ reacts with $ZnAl_2O_4$ and SiO_2 to form $SrAl_2Si_2O_8$, TiO_2 and Zn_2SiO_4 at y = 0.2 to 0.8, and SiO_2 phase disappears at y = 0.8; new phase of Zn_2TiO_4 is obtained at y = 1. The existence of TiO_2 has important effect on the dielectric properties. The optimized microwave dielectric properties are obtained at y = 0.6 and the ceramics show low dielectric constant (7.16), high-quality factor (57, 837 GHz), and low temperature coefficient of resonant frequency (−30 ppm °C^{-1}).

1. Introduction

With the development of the fifth generation mobile communication technology (5G), millimeter-wave frequencies become the preferred carrier frequencies because of broader bandwidth and faster transmission rate [1,2]. For millimeter-wave technology, ceramic substrates have obvious advantages due to their ultra-low dielectric loss, stable and adjustable dielectric constant and stable temperature characteristics [3,4]. For substrate application especially in the future generation of microwave integrated circuit (MIC), low dielectric constant is very important because it yields higher signal propagation velocity and it can also reduce inductive crosstalk and noise generation in the MIC [5,6].

According to the Clausius-Mossotti equation, the dielectric constant is mainly determined by the dielectric polarizability per volume [7]. The dielectric polarizability of compound can be predicated from ion polarizability using additivity rule [8]. To get low dielectric constant, the ion with low polarizability is favored. As reported by Shannon [8], there are only four ions of Be^{2+}, B^{3+}, Al^{3+}, Si^{4+} with polarizability less than one. Among them, the compounds containing Al^{3+} [9] or Si^{4+} attracted a great attention for substrate application due to their low dielectric constant, high quality factor, environment friendly, low cost and good mechanical properties, such as Zn_2SiO_4 (ε_r = 6.6, $Q \times f$ = 219,000 GHz, τ_f = −61 ppm °C^{-1}) [6] and $ZnAl_2O_4$ (ε_r = 8.5, $Q \times f$ = 56,319 GHz, τ_f = −79 ppm °C^{-1}) [10]. However, high sintering temperature of Zn_2SiO_4 and $ZnAl_2O_4$ leads to the evaporation of zinc and the instability of dielectric performances [11]. Moreover, the dielectric constant of modified aluminate and silicate with near-zero τ_f such as Zn_2SiO_4–TiO_2 (ε_r = 9.3) [6] and $ZnAl_2O_4$–TiO_2 (ε_r = 12.67) [10] still needs to be reduced.

Both $ZnAl_2O_4$ (gahnite) and Zn_2SiO_4 (willemite) are binary compounds in the ternary ZnO–Al_2O_3–SiO_2 system [12,13]. Willemite (Zn_2SiO_4) was found to melt congruently at 1512 °C and gahnite ($ZnAl_2O_4$) melts congruently at temperatures close to 1950 °C. The binary eutectic between willemite and gahnite was reported to be at 1460 °C and the ternary eutectic involving willemite and gahnite was found to be at 1315 °C in the $ZnAl_2O_4$–Zn_2SiO_4–SiO_2 system. Usually, the sintering temperature of compounds is closely related to their melting point. It is meaningful to investigate microwave dielectric properties of ceramics in $ZnAl_2O_4$–Zn_2SiO_4–SiO_2 system for the low ternary eutectic point and low dielectric constant.

Considering the negative temperature coefficient of resonant frequency (τ_f) for Zn_2SiO_4 and $ZnAl_2O_4$, compound of positive τ_f should be incorporated to get near-zero τ_f. Generally, the Ti-based ceramic materials, such as TiO_2 [10,14], $CaTiO_3$ [15,16] and $SrTiO_3$ [17,18], are used to compensate the negative τ_f value of microwave dielectric ceramics. In present work, $SrTiO_3$ is incorporated into $ZnAl_2O_4$–Zn_2SiO_4–SiO_2 ceramic and the microwave dielectric properties are investigated together with the phase evolution and sintering characteristics.

* Corresponding author.
E-mail address: Huxing@scut.edu.cn (X. Hu).

https://doi.org/10.1016/j.ceramint.2019.11.196
Received 6 October 2019; Received in revised form 14 November 2019; Accepted 22 November 2019

2. Experimental

High-purity powders (≥99.9%) of Al_2O_3, ZnO, fused SiO_2 and $SrTiO_3$ were used as the starting materials, weighed in a stoichiometric ratio and ball milled in ethanol with zirconia balls for 1 h [19]. $ZnAl_2O_4$–$3Zn_2SiO_4$-$xSiO_2$ (x = 0, 2, 4, 6) powders were synthesized using the conventional solid-state reaction method by calcining in an alumina crucible at 1150 °C for 3 h. Those calcined powders were ground into fine powders and remilled with $SrTiO_3$ according to the desired stoichiometry $ZnAl_2O_4$–$3Zn_2SiO_4$–$2SiO_2$-$ySrTiO_3$ (y = 0, 0.2, 0.4, 0.6, 0.8, 1) with the same condition in previous process. The dried powders, with 6 wt% PVA (polyvinyl alcohol) added, were pressed into rods of 10 mm diameter and 5 mm thickness under a pressure of 20,000 psi and these compacts were sintered at temperatures from 1150 °C to 1450 °C in air for 3 h.

Phase constitutions were identified by X-ray diffraction (XRD) patterns using CuKα radiation (Rigaku D/max-IIIA, Tokyo, Japan). The bulk densities of the sintered bodies were determined by the Archimedes method. The morphologies of the polished ceramics were examined with a ZEISS EVO 18 tungsten wire filament scanning electron microscope and the EDS analysis was also performed (Carl Zeiss Jena, Oberkochen, Germany). The microwave dielectric properties were evaluated by Hakki and Coleman's resonator method (Agilent E8363B network analyzer, Santa Clara, CA). The temperature coefficient of resonant frequency (τ_f) was estimated from Eq. (1) [19,20] where α is the linear expansion coefficient (α = ~10 ppm°C^{-1}), and τ_ε is the temperature coefficient of dielectric constant evaluated at 1 MHz by an LCR meter (HP 4288A; Agilent) equipped with a thermostat range from −55 °C to 125 °C.

$$\tau_f\ (\text{ppm}\ ^\circ\text{C}^{-1}) = -(\alpha + 0.5\tau_\varepsilon) \quad (1)$$

3. Results and discussion

According to the desired stoichiometry $ZnAl_2O_4$–$3Zn_2SiO_4$-$xSiO_2$ (x = 0, 2, 4, 6), the mixture of ZnO, Al_2O_3 and fused SiO_2 was calcined at 1150 °C for 3 h and the ceramic was sintered at 1280–1450 °C. The dense $ZnAl_2O_4$–$3Zn_2SiO_4$ ceramic (density: 4.49 g cm^{-3}) is obtained at sintering temperature of 1380 °C and the dense $ZnAl_2O_4$–$3Zn_2SiO_4$–$2SiO_2$ ceramic (density: 3.92 g cm^{-3}) is obtained at sintering temperature of 1320 °C which is 60 °C less than that for dense $ZnAl_2O_4$–$3Zn_2SiO_4$ ceramic. The $ZnAl_2O_4$–$3Zn_2SiO_4$–$2SiO_2$ ceramic sintered at 1340 °C shows crack when cooling to room temperature because of the phase transition of crystalline SiO_2 [21]. The relative density of $ZnAl_2O_4$–$3Zn_2SiO_4$–$2SiO_2$ ceramic is more than 98% considering the theory density of $ZnAl_2O_4$ (4.61 g cm^{-3}), Zn_2SiO_4 (4.25 g cm^{-3}) and fused SiO_2 (~2.2 g cm^{-3}). Unfortunately, dense ceramic of $ZnAl_2O_4$–$3Zn_2SiO_4$–$4SiO_2$ and $ZnAl_2O_4$–$3Zn_2SiO_4$–$6SiO_2$ are not obtained.

The XRD results of calcined powders according to $ZnAl_2O_4$–$3Zn_2SiO_4$–$2SiO_2$ are shown in Fig. 1. Both $ZnAl_2O_4$ and Zn_2SiO_4 phase are found in Fig. 1 and no diffraction peaks of SiO_2 are found because of the amorphous characteristics of the fused silica. When $SrTiO_3$ is incorporated into $ZnAl_2O_4$–$3Zn_2SiO_4$–$2SiO_2$, the sintering temperature corresponding to dense ceramic is reduced to ~1200 °C. The XRD patterns of ceramics sintered at 1200°Caccording to the desired stoichiometry $ZnAl_2O_4$–$3Zn_2SiO_4$–$2SiO_2$-$ySrTiO_3$ are shown in Fig. 2. The XRD results are shown as follows: Zn_2SiO_4 phase is found in all compositions; the intensity of diffraction for $ZnAl_2O_4$ phase gradually decreases until it disappears when y = 1; the perovskite phase of $SrTiO_3$ is not found in all composition; the crystalline SiO_2 is still not found in all compositions; new phase of strontium feldspar ($SrAl_2Si_2O_8$: PDF number 38–1454) is found when y = 0.2 to 1; when y = 1, Zinc Titanate (Zn_2TiO_4: PDF number 25–1164) is found and the diffraction peak of $ZnAl_2O_4$ is disappeared.

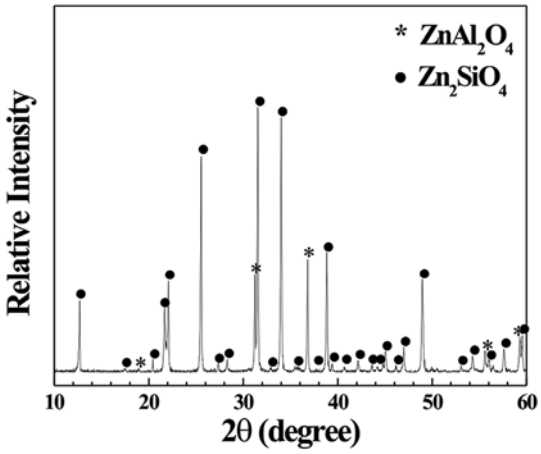

Fig. 1. XRD patterns of $ZnAl_2O_4$–$3Zn_2SiO_4$–$2SiO_2$ calcined at 1150 °C for 3 h.

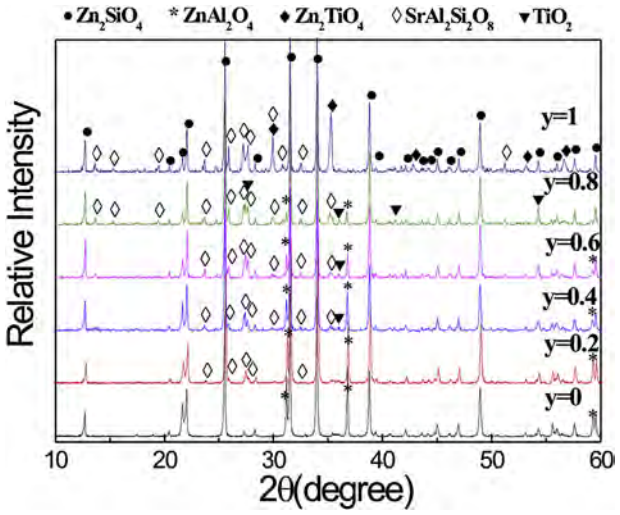

Fig. 2. XRD patterns of $ZnAl_2O_4$–$3Zn_2SiO_4$–$2SiO_2$–$ySrTiO_3$ ceramics.

For strontium feldspar phase, Sr ion comes from $SrTiO_3$ and Al ion comes from $ZnAl_2O_4$. The remnant Ti ion in $SrTiO_3$ could be in the form of rutile phase TiO_2 or it could react with the remnant Zinc from $ZnAl_2O_4$ to form Zinc Titanate. When y = 0.2 to 0.8, the strongest diffraction peak of (110) plane at 27.4° in rutile phase is overlapped with the diffraction peaks of strontium feldspar and the second strongest diffraction peak of (211) plane at 54.3° in rutile phase is overlapped with the diffraction peak of Zinc Silicate. The diffraction peaks of (111) plane and (210) plane at 41.2° and 44.1° indicate the existence of rutile phase when y = 0.8. As shown in enlarged part of diffraction peak (Fig. 3), the split peak (as shown by arrow) at 27.4° is also attributed to the diffraction peak of (110) plane in rutile phase.

To reveal the phase revolution of $SrTiO_3$ added ceramic, back scattering electron (BSE) images of the polished surfaces are presented in Fig. 4. As shown in Fig. 4a, light gray regions (Zn_2SiO_4), gray regions ($ZnAl_2O_4$) and black regions (SiO_2) are observed and the compositions are confirmed by the EDX spot analysis. For $SrTiO_3$ added ceramic such as y equals from 0.2 to 0.6, finer microstructures with multi-phases are obtained. The dark gray regions are found and they are identified to Sr feldspar phase by the EDX spot analysis. When y = 1, white color regions are found and they are attributed to Zn_2TiO_4 phase from EDX results. However, the Ti based phase is failed to be identified by BSE images and EDX spot analysis when y = 0.2 to 0.8. Considering that the brightness contrast for BSE images is closely related to the average element number (AEN) of compounds [22], it is difficult to distinguish rutile phase (AEN: 12.67) from $ZnAl_2O_4$ phase (AEN: 12.57) in the BSE

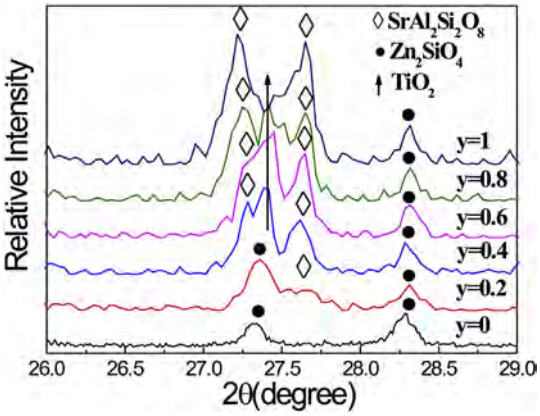

Fig. 3. Magnified XRD patterns of $ZnAl_2O_4$–$3Zn_2SiO_4$–$2SiO_2$–$ySrTiO_3$ ceramics in the range 26˚–29˚.

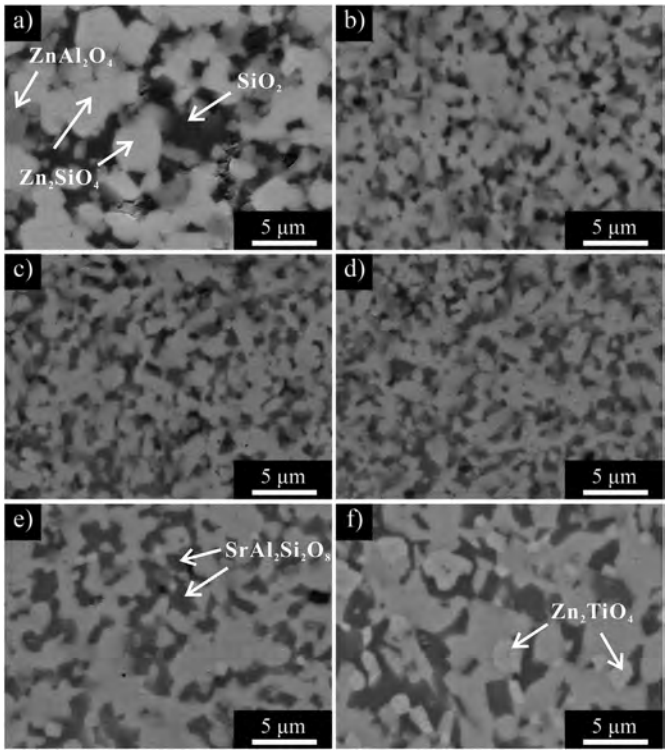

Fig. 4. BSE micrographs of $ZnAl_2O_4$–$3Zn_2SiO_4$–$2SiO_2$-$ySrTiO_3$ ceramics: (a) y = 0, sintered at 1320 ˚C; (b) y = 0.2, sintered at 1180 ˚C; (c) y = 0.4, sintered at 1180 ˚C; (d) y = 0.6, sintered at 1180 ˚C; (e) y = 0.8, sintered at 1200 ˚C; (f) y = 1, sintered at 1200 ˚C.

images.

To reveal the distribution of Ti element, the corresponding elemental mapping images are shown in Fig. 5 and Fig. 6. The mapping results show that Ti element is homogeneously distributed for y = 0.8. The brighter contrast regions for Ti element in Fig. 5b (such as circled in white) are in accordance with the darker contrast regions in Fig. 5c and d (such as circled in white). The results show no formation of compounds between Ti and Zn or Sr element. The EDX spot analysis on the brighter contrast region confirms the existence of TiO_2-rich phase (not shown here). Considering the previous XRD results, the most possible phase including Ti element is TiO_2 for y = 0.8.

For y = 1, the brighter contrast regions for Ti element in Fig. 6b are in accordance with the darker contrast region for Zn element in Fig. 6c and Sr element in Fig. 6d (circled in white) and the TiO_2 phase is identified by the EDX spot analysisas shown in Fig. 6e. Some bright

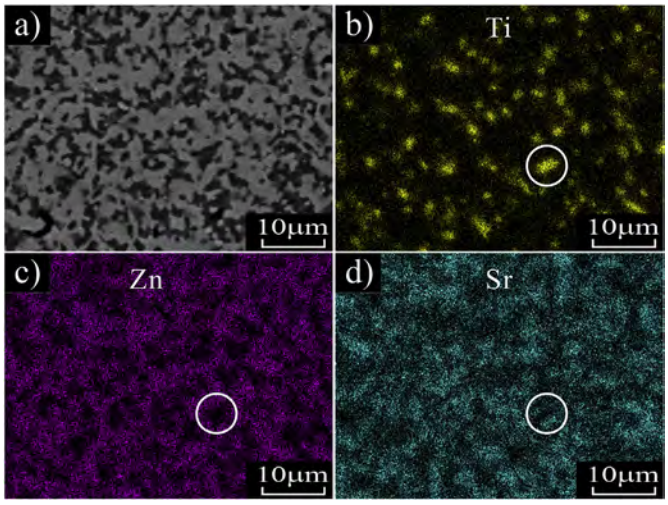

Fig. 5. BSE micrographs (a) and EDX elemental mapping images (b–d) showing elemental distributions of Ti, Zn and Sr in $ZnAl_2O_4$–$3Zn_2SiO_4$–$2SiO_2$-$0.8SrTiO_3$ ceramics.

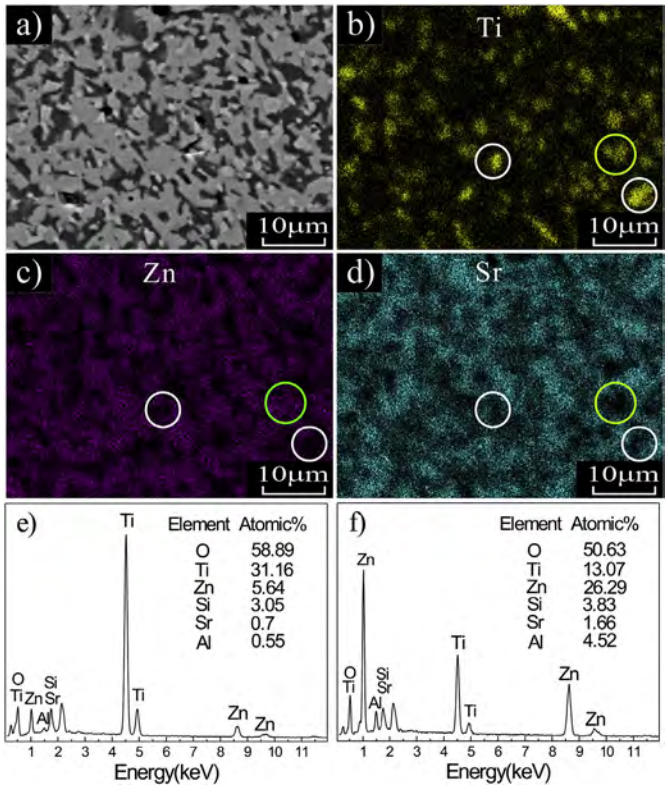

Fig. 6. BSE micrographs (a) and EDX elemental mapping images (b–d) showing elemental distributions of Ti, Zn and Sr in $ZnAl_2O_4$–$3Zn_2SiO_4$–$2SiO_2$–$SrTiO_3$ ceramics; EDX spot analysis results (e–f) on the different brighter contrast region for Ti element.

contrast regions for Ti element in Fig. 6a are in accordance with the brighter contrast regions for Zn element in Fig. 6c and the darker contrast region for Sr element in Fig. 6d (circled in green), and the phase is attributed to Zn_2TiO_4 which is confirmed by the EDX spot analysis as shown in Fig. 6f in accordance with XRD results.

From XRD results and B-SEM, the phase evolution is suggested as shown in equations (2)–(6).

$$ZnAl_2O_4 + 3Zn_2SiO_4 + 2SiO_2 + 0.2SrTiO_3 \rightarrow$$
$$0.8ZnAl_2O_4 + 3.1Zn_2SiO_4 + 1.5SiO_2 + 0.2SrAl_2Si_2O_8 + 0.2TiO_2 \quad (2)$$

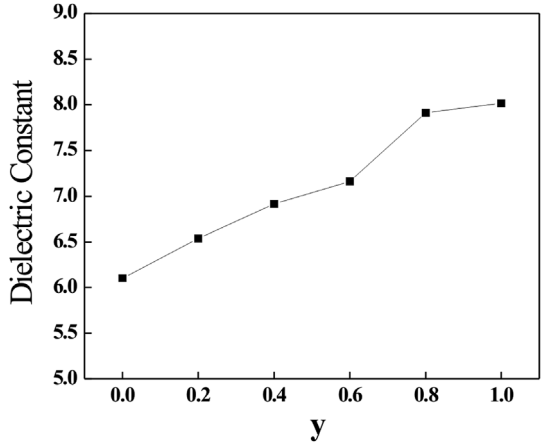

Fig. 7. Dielectric constant as a function of y in $ZnAl_2O_4$–$3Zn_2SiO_4$–$2SiO_2$-y$SrTiO_3$ ceramics.

$$ZnAl_2O_4 + 3Zn_2SiO_4 + 2SiO_2 + 0.4SrTiO_3 \rightarrow 0.6ZnAl_2O_4 + 3.2Zn_2SiO_4 + SiO_2 + 0.4SrAl_2Si_2O_8 + 0.4TiO_2 \quad (3)$$

$$ZnAl_2O_4 + 3Zn_2SiO_4 + 2SiO_2 + 0.6SrTiO_3 \rightarrow 0.4ZnAl_2O_4 + 3.3Zn_2SiO_4 + 0.5SiO_2 + 0.6SrAl_2Si_2O_8 + 0.6TiO_2 \quad (4)$$

$$ZnAl_2O_4 + 3Zn_2SiO_4 + 2SiO_2 + 0.8SrTiO_3 \rightarrow 0.2ZnAl_2O_4 + 3.4Zn_2SiO_4 + 0.8SrAl_2Si_2O_8 + 0.8TiO_2 \quad (5)$$

$$ZnAl_2O_4 + 3Zn_2SiO_4 + 2SiO_2 + SrTiO_3 \rightarrow 3Zn_2SiO_4 + SrAl_2Si_2O_8 + 0.5TiO_2 + 0.5Zn_2TiO_4 \quad (6)$$

When y = 0.2 to 0.8, $SrTiO_3$ reacts with $ZnAl_2O_4$ and SiO_2, then $SrAl_2Si_2O_8$, Zn_2SiO_4 and TiO_2 are obtained; when y = 0.8, all the SiO_2 phases disappear after providing Si source in feldspar phase and reacting with Zn ion from $ZnAl_2O_4$; when y = 1, all the SiO_2 phase just can meet the demand of feldspar for Si source and the remnant Zn ion from $ZnAl_2O_4$ reacts with part of TiO_2 phase to get Zn_2TiO_4 phase.

Phase evolution always has important influence on dielectric properties. Fig. 7 shows the relation between the dielectric constant of ceramics and the addition amount of $SrTiO_3$. For each composition, the sintering temperature corresponding to the highest bulk density is chosen for the investigation of dielectric properties. As shown in Fig. 7, with the increase of $SrTiO_3$ content, the dielectric constant of ceramics gradually increases. When y increases from 0 to 0.8, the increasing dielectric constant is due to the increasing amount of rutile phase which has a high dielectric constant of 100 [23]. When y = 1, though Zn_2TiO_4 has higher dielectric constant than that of SiO_2, Zn_2SiO_4 and $ZnAl_2O_4$, the dielectric constant of ceramic increases slowly due to the decrease of TiO_2 phase amount.

Fig. 8 demonstrates the temperature dependence of capacitance change based on the capacitance at 25 °C for $ZnAl_2O_4$–$3Zn_2SiO_4$–$2SiO_2$–y$SrTiO_3$ ceramics. In all the compositions, the dielectric constant increases with the increasing temperature. With the increasing content of $SrTiO_3$, the temperature coefficient of dielectric constant decreases first from y = 0 to 0.6, and then it increases from y = 0.8 to 1. The temperature coefficient of ceramic is close related to the content of rutile phase. With increasing y from 0 to 0.6, the decreasing temperature coefficient is due to the increasing rutile phase which has a large negative temperature coefficient of dielectric constant (−750 ppm °C^{-1}) [24]. With increasing y from 0.8 to 1, the rutile phase decreases and then temperature coefficient of dielectric constant increases.

The microwave dielectric properties are given in Table 1. The ceramic with y = 0.8 has the highest Q × f value. The lower Qf value for y = 1 is due to the existence of Zn_2TiO_4 phase. Golovchansky et al. has reported microwave dielectric properties of Zn_2TiO_4: ε_r = 15, $Q \times f$ = 2200 GHz, τ_f = −28 ppm °C^{-1} [25]. Sr feldspar has also low dielectric constant, and the existence of Sr feldspar (ε_r = 3.56) [26] is helpful to keep ceramic the low dielectric constant and high Q value [24]. The multiphase system is also helpful to obtain lower sintering temperature in present system, compared to that of $ZnAl_2O_4$–TiO_2–$SrAl_2Si_2O_8$ system. The optimized composition for that system is 0.7(0.75$ZnAl_2O_4$-0.25TiO_2)-0.3$SrAl_2Si_2O_8$ ceramic sintered at 1550 °C, which has microwave properties: ε_r = 7.32, $Q \times f$ = 27,130 GHz, τ_f = +2.98 ppm °C^{-1} [26]. The optimized microwave dielectric properties in present system is obtained as follows: y = 0.6, ε_r = 7.16, $Q \times f$ = 57,837 GHz, τ_f = −30 ppm°C^{-1}, sintered at 1200 °C; y = 0.8, ε_r = 7.91, $Q \times f$ = 61, 607 GHz, τ_f = −35 ppm°C^{-1}, sintered at 1180 °C.

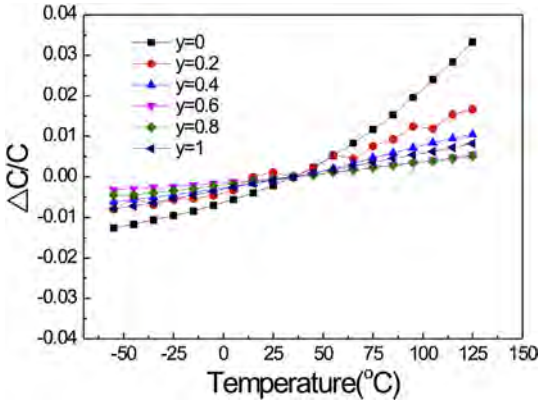

Fig. 8. Temperature dependence of capacitance change for $ZnAl_2O_4$–$3Zn_2SiO_4$–$2SiO_2$-y$SrTiO_3$ ceramics.

Table 1
Microwave dielectric properties of $ZnAl_2O_4$–$3Zn_2SiO_4$–$2SiO_2$-y$SrTiO_3$ ceramics.

y	Sintering Temperature (°C)	ε_r	$Q \times f$ (GHz)	τ_f(ppm °C^{-1})
0	1300	6.11	36103	−97
0.2	1200	6.54	54383	−62
0.4	1180	6.89	42582	−49.5
0.6	1180	7.16	57837	−30
0.8	1200	7.91	61607	−35
1	1200	8.01	39759	−53

4. Conclusions

In present work, $SrTiO_3$ added $ZnAl_2O_3$–$3Zn_2SiO_4$–$2SiO_2$ ceramics were fabricated by solid-state reaction method. With the addition of $SrTiO_3$, the sintering temperature for dense ceramic is reduced from 1320 °C to 1180–1200 °C. According to the nominal composition Zn_2SiO_4–$3ZnAl_2O_4$–$2SiO_2$-y$SrTiO_3$, phase evolution is revealed by XRD patterns and Back Scattering Electron images: when y = 0.2 to 0.8, $SrTiO_3$ reacts with $ZnAl_2O_4$ and SiO_2, then $SrAl_2Si_2O_8$, Zn_2SiO_4 and TiO_2 are obtained; when y = 0.8, all the SiO_2 phases disappear after providing Si source in feldspar phase and reacting with Zn ion from $ZnAl_2O_4$; when y = 1, all the SiO_2 phases contribute to formation of feldspar and the remnant Zn ion from $ZnAl_2O_4$ reacts with part of TiO_2 phase to get Zn_2TiO_4 phase. The amount of TiO_2 phase has important effect on the dielectric constant and the temperature coefficient of dielectric constant. The optimized microwave dielectric properties in present system is obtained as follows: y = 0.6, ε_r = 7.16, $Q \times f$ = 57, 837 GHz, τ_f = −30 ppm°C^{-1}, sintered at 1200 °C; y = 0.8, ε_r = 7.91, $Q \times f$ = 61, 607 GHz, τ_f = −35 ppm°C^{-1}, sintered at 1180 °C.

Declaration of competing interest

We declare that we have no known competing financial interests or

personal relationships that could have appeared to influence the work reported in this paper.

Acknowledgements

This work was supported by Guangzhou Nova Program (2012J2200013).

References

[1] M. Agiwal, A. Roy, N. Saxena, Next generation 5G wireless networks: a comprehensive survey, IEEE Commun. Surv. Tut. 18 (3) (2016) 1617–1655.
[2] T.S. Rappaport, S. Sun, R. Mayzus, H. Zhao, Y. Azar, K. Wang, G.N. Wong, J.K. Schulz, M. Samimi, F. Gutierrez, Millimeter wave mobile communications for 5G cellular: it will work!, IEEE Access 1 (2013) 335–349.
[3] I.M. Reaney, D. Iddles, Microwave dielectric ceramics for resonators and filters in mobile phone networks, J. Am. Ceram. Soc. 89 (7) (2006) 2063–2072.
[4] R.J. Cava, Dielectric materials for applications in microwave communications, J. Mater. Chem. 11 (2001) 54–62.
[5] L. Li, W.B. Hong, G.Y. Chen, X.M. Chen, High-performance (1-x)($0.2B_2O_3$-$0.8SiO_2$)-$xTiO_2$ (x = 0.025-0.1) glass matrix composites for microwave substrate applications, J. Alloy. Comp. 774 (2019) 706–709.
[6] Y. Guo, H. Ohsato, K.I. Kakimoto, Characterization and dielectric behavior of willemite and TiO2-doped willemite ceramics at millimeter-wave frequency, J. Eur. Ceram. Soc. 26 (10–11) (2006) 1827–1830.
[7] R. Roberts, Polarizabilities of ions in perovskite type crystals, Phys. Rev. 81 (1951) 865–868.
[8] R.D. Shannon, Dielectric polarizabilities of ions in oxides and fluorides, J. Appl. Phys. 73 (1) (1993) 348–366.
[9] L. Yi, M.M. Mao, L. Li, X.M. Chen, Structures and microwave dielectric characteristics of compounds in vicinity of $CaNdAlO_4$ in CaO-Nd_2O_3-Al_2O_3 tenary system, Adv. Appl. Ceram. 112 (1) (2013) 46–52.
[10] K.P. Surendran, N. Santha, P. Mohanan, M.T. Sebastian, Temperature stable low loss ceramic dielectrics in (1-x)$ZnAl_2O_4$-$xTiO_2$ system for microwave substrate applications, Eur. Phys. J. B 41 (3) (2004) 301–306.
[11] W. Wang, L.J. Tang, W.F. Bai, B. Shen, J.W. Zhai, Microwave dielectric properties of (1-x)$(Mg_{0.4}Zn_{0.6})_2SiO_4$–x$CaTiO_3$ composite ceramics, J. Mater. Sci. Mater. Electron. 25 (2014) 3601–3607.
[12] E.N. Bunting, System ZnO-Al_2O_3-SiO_2, Res J. Natl. Bur. Stand. 8 (2) (1932) 279–287.
[13] R. Hansson, B.J. Zhao, P.C. Hayes, E. Jak, A reinvestigation of phase equilibria in the system Al_2O_3-SiO_2-ZnO, Metall. Mater. Trans. B 36 (2) (2005) 187–193.
[14] Z.Z. Weng, C.X. Song, Z.X. Xiong, H. Xue, W.F. Sun, Y. Zhang, B. Yang, M.J. Reece, H.X. Yan, Micostructure and broadband dielectrics of Zn_2SiO_4 ceramics with nano-sized TiO_2 addition, Ceram. Int. 45 (10) (2019) 13251–13256.
[15] X. Hu, X.M. Chen, X.J. Lu, Temperature-stable dielectric ceramics in $Pb(Mg_{1/3}Nb_{2/3})O_3$-$CaTiO_3$-$Bi_4Ti_3O_{12}$ pseudo-ternary system, Ceram. Int. 28 (1) (2002) 69–73.
[16] Z.Z. Weng, R.G. Guan, Z.X. Xiong, Effects of the ZBS addition on the sintering behavior and microwave dielectric properties of $0.95Zn_2SiO_4$-$0.05CaTiO_3$ ceramics, J. Alloy. Comp. 695 (2017) 3517–3521.
[17] C.E. Huang, X.R. Lu, M.Y. Lu, Y. Huan, Effect of CaO/SnO2 additives on the microstructure and microwave dielectric properties of $SrTiO_3$-$LaAlO_3$ ceramics, Ceram. Int. 43 (13) (2017) 10624–10627.
[18] C.L. Huang, J.Y. Chen, C.C. Liang, Dielectric properties and mixture behavior of $Mg_4Nb_2O_9$-$SrTiO_3$ ceramic system at microwave frequency, J. Alloy. Comp. 478 (2009) 554–558.
[19] Z.F. Cheng, X. Hu, Y. Li, Z.Y. Ling, Fabrication and microwave dielectric properties of Mg_2SiO_4-$LiMgPO_4$-TiO_2 Composite Ceramics, J. Am. Ceram. Soc. 99 (8) (2016) 2688–2692.
[20] P.J. Harrop, Temperature coefficients of capacitance of solids, J. Mater. Sci. 4 (1969) 370–374.
[21] Y. Fang, L. Li, Q. Xiao, X.M. Chen, Preparation and microwave dielectric properties of cristobalite ceramics, Ceram. Int. 38 (2012) 4511–4515.
[22] M.G. Hall, G.E. Lloyd, The SEM examination of geological samples with a semiconductor back-scattered electron detector, Am. Mineral. 66 (1981) 362–368.
[23] A. Templeton, X. Wang, S.J. Penn, S.J. Webb, L.F. Cohen, N.M. Alford, Microwave dielectric loss of titanium oxide, J. Am. Ceram. Soc. 83 (2000) 95–100.
[24] S.X. Dai, R.F. Huang, D.L. Wilcox, Use of titanates to achieve a temperature-stable low-temperature cofired ceramic dielectric for wireless applications, J. Am. Ceram. Soc. 85 (4) (2002) 828–832.
[25] A. Golovchansky, H.T. Kim, Y. Kim, Zinc titanates dielectric ceramics prepared by sol-gel process, J. Korean Phys. Soc. 32 (1998) S1167–S1169.
[26] X.C. Wang, W. Lei, R. Ang, W.Z. Lu, $ZnAl_2O_4$–TiO_2–$SrAl_2Si_2O_8$ low-permittivity microwave dielectric ceramics, Ceram. Int. 39 (2013) 1707–1710.